Advances in Water Resources 60 (2013) 89–99

Contents lists available at ScienceDirect

Advances in Water Resources

journal homepage: www.elsevier.com/locate/advwatres

The Analytic Element Method for rectangular gridded domains, benchmark comparisons and application to the High Plains Aquifer ☆

David R. Steward *, Andrew J. Allen

Department of Civil Engineering, Kansas State University, 2118 Fiedler Hall, Manhattan, KS 66506 5000, USA

ARTICLE INFO

Article history:
Received 31 January 2013
Received in revised form 8 July 2013
Accepted 12 July 2013
Available online 27 July 2013

Keywords:
Analytic Element Method
Separation of variables
Laplace equation
Groundwater
Heterogeneity
High Plains Aquifer

ABSTRACT

Groundwater studies face computational limitations when providing local detail (such as well drawdown) within regional models. We adapt the Analytic Element Method (AEM) to extend separation of variable solutions for a rectangle to domains composed of multiple interconnected rectangular elements. Each rectangle contains a series solution that satisfies the governing equations and coefficients are adjusted to match boundary conditions at the edge of the domain and continuity conditions across adjacent rectangles. A complete mathematical implementation is presented including matrices to solve boundary and continuity conditions. This approach gathers the mathematical functions associated with head and velocity within a small set of functions for each rectangle, enabling fast computation of these variables. Benchmark studies verify that conservation of mass and energy conditions are accurately satisfied using a method of images solution, and also develop a solution for heterogeneous hydraulic conductivity with log normal distribution. A case study illustrates that the methods are capable of modeling local detail within a large-scale regional model of the High Plains Aquifer in the central USA and reports the numerical costs associated with increasing resolution, where use is made of GIS datasets for thousands of rectangular elements each with unique geologic and hydrologic properties, Methods are applicable to interconnected rectangular domains in other fields of study such as heat conduction, electrical conduction, and unsaturated groundwater flow.

1. Introduction

Groundwater problems may be formulated as boundary value problems using separation of variables. The basis for this method was established by Fourier [17], who summed Fourier series multiplied by exponential functions to study the steady propagation of heat in a rectangular solid. Separation of variables has evolved into a powerful method to solve problems in domains bounded by natural coordinates, where solutions are obtained by summing series solutions to the governing differential equations [1]. Solutions exist for domains with the geometry of rectangles, circles, parabolas, hyperbolas, spheres, and ellipsoids [29,30], The specific geometry of rectangular domains is important in the fields of heat conduction [8], electrical conduction [40], and unsaturated groundwater flow [26].

While separation of variables has been successfully applied to the problem of a single isolated rectangular domain, important problems exist for grids of adjacent, interconnected rectangles. Our case study contains thousands of rectangles, each with unique properties associated with the geologic medium and surficial fluxes. An existing numerical approach to solving problems on a rectangular gridded domain is application of the finite difference method [28], which gives the value of a function at the set of grid points and utilizes an interpolation scheme to obtain its value throughout the domain. Another approach that captures the functional variation across rectangular elements uses Cauchy integrals at the intersections of every rectangle [25,31]. Computational challenges exist with Cauchy integrals when domains become large and the number of mathematical functions increase.

Recent groundwater developments in the Analytic Element Method have enabled separation of variables solutions for individual elements to be superimposed for modeling domains with multiple elements. Mathematical developments in a one-layer aquifer for fully saturated, steady groundwater flow was first presented by [7] for the geometry of circles, by [44] for ellipses, and by [22] for spheroids. Such geometries have been extended in many studies to mutilayer aquifers, unsaturated flow and unsteady flow, and methods also exist for connected domains with curved boundaries [5,12]. However, the geometry of such elements cannot intersect or overlap, and solutions to the Embedded Matrix Method place the individual elements into a homogeneous background [15]. Sep-

* Corresponding author. Tel.: +1 (785) 532 1585.
E-mail addresses: steward@ksu.edu (D.R. Steward), andya@ksu.edu (A.J. Allen).

0309-1708/$ - see front matter © 2013 The Authors. Published by Elsevier Ltd. All rights reserved.
http://dx.doi.org/10.1016/j.advwatres.2013.07.009

aration of variables is advantageous in that it very accurately reproduces local boundary conditions within a regional setting, typically an infinite domain. This approach also faces the computational challenge associated with increasing evaluation time with increasing mathematical complexity.

One method to resolve the numerical challenge associated with evaluating a large number of Cauchy integrals and separation of variables solutions is based upon the superblock approach [43]. Here, the mathematical functions for individual features are gathered into families of elements, each with a more computationally efficient series expansions for evaluation at larger distances from a group of features. The computational advantage of superblocks has been demonstrated for regional modeling with Cauchy integrals [13], for separation of variables with circles and spheroids [23,24], and for functions associated with groundwater uptake by fields of phreatophytes [34]. However, the superblock approach does not explicitly allow for jump in aquifer properties between different domains. Another approach to dealing with mathematical complexity was developed by [16] who grouped elements into subdomains and then utilized Cauchy integrals to match continuity conditions at subdomain boundaries. This method results in a set of polygon subdomain models, each with their own individual solution.

We develop new methods to solve boundary value problems for domains with interconnected rectangles by extending the Analytic Element Method (AEM) to existing, common methods associated with separation of variables (SOV) for a single, isolated rectangle. This gathers the mathematical functions for all features into families of rectangular elements, and evaluation of functions only requires computation of those associated with an individual rectangle, similar to the Cauchy integral subdomain approach of [16]. This solution also enables rectangular heterogeneities to adjoin along common boundaries and completely fill a domain. The mathematical development is presented next in the methods section; then benchmark studies compare the solution to that obtained using the method of images and also develop a model of rectangular heterogeneities with log normal conductivity distribution; and finally a case study illustrates its application to study an important groundwater problem spanning the High Plains Aquifer region of southwestern Kansas.

2. Methods

Mathematical development is presented here within a framework called the Analytic Element Method (AEM), which was invented by Strack [41,42]. Our adaptation of the AEM comprises a four-step process:

1. Divide the problem domain into analytic elements with boundaries of prescribed geometry.
2. Develop a set of influence functions that satisfy the partial differential equation and allow variation along an element with forms capable of unique solutions.
3. Build a comprehensive solution comprised of linear solutions of influence functions for each element times a priori unknown coefficients, and
4. Develop a solution algorithm to adjust coefficients to match boundary conditions.

Development of these methods for gridded rectangular domains is presented next.

2.1. Rectangular elements on a gridded domain

Boundary value problems in domains composed of rectangular grids are specified as follows. First, the domain is subdivided into rectangular elements bounded by grid lines in the Cartesian coordinate system as illustrated in Fig. 1. The values of x and y are specified for each element to take on constant values of x_1 on side 1, y_1 on side 2, x_2 on side 3 and y_2 on side 4. The particular geometry identified in Fig. 1a is used later to illustrate application of the methods to the groundwater field of study. This geometry with grids of interconnected rectangles are common to the underlying GIS raster data (as shown later in Fig. 4), obtained through spatial analysis of the underlying data sets.

2.2. Influence functions for an element

The two primary variables used to represent solutions to groundwater problems are related to the groundwater discharge and elevation measured as head h. Groundwater flow occurs within an aquifer layer with base elevation B, thickness H, and hydraulic conductivity k. Governing equations may be represented in terms of a potential function

$$\Phi = \begin{cases} \frac{1}{2}k(h-B)^2 & 0 \leqslant (h-B) \leqslant H \\ kH(h-B) - \frac{kH^2}{2} & H \leqslant (h-B) \end{cases} \tag{1}$$

where this relation takes on different forms for unconfined and confined conditions [19,41]. Steady groundwater flow satisfies the Poisson equation

$$\frac{\partial^2\Phi}{\partial x^2} + \frac{\partial^2\Phi}{\partial y^2} = -R \tag{2}$$

where R is the rate of recharge into the aquifer layer. The groundwater velocity is quantified using the discharge per width obtained from minus the gradient of the potential function:

$$\mathbf{Q} = -\nabla\Phi \tag{3}$$

Dirichlet boundary conditions with given head are specified in terms of the potential using (1) and Neumann conditions specify the normal component of the discharge per width, $Q_{\hat{n}} = -\partial\Phi/\partial\hat{n}$. Once a solution is obtained in terms of Φ, the head is obtained by inverting (1):

$$h = B + \begin{cases} 0 & \Phi \leqslant 0 \\ \sqrt{\frac{2\Phi}{k}} & 0 \leqslant \Phi \leqslant \frac{kH^2}{2} \\ \frac{\Phi}{kH} + \frac{H}{2} & \frac{kH^2}{2} \leqslant (h-B) \end{cases} \tag{4}$$

Note that the $\Phi < 0$ case is considered, since during iteration before a solution is achieved the potential may become negative, and yet physically the head cannot go below the base elevation of an aquifer [33].

In separation of variables, the function Φ is expressed in the form

$$\Phi(x,y) = X(x)Y(y) \tag{5}$$

where X varies only as a function of x and Y is a function of y. Substituting this form in the Laplace equation

$$\frac{\partial^2\Phi}{\partial x^2} + \frac{\partial^2\Phi}{\partial y^2} = 0 \tag{6}$$

leads to the following set of ordinary differential equations [29,30]

$$\begin{aligned} \tfrac{d^2X}{dx^2} &= \pm pX \\ \tfrac{d^2Y}{dy^2} &= \mp pY \end{aligned} \tag{7}$$

with solutions composed of $\cos, \sin, \cosh$ and $\sinh$ functions of x, y and the constant p. The potential Φ is obtained by linear combinations of these functions in (5).

For the rectangular element in Fig. 1b, we formulate the separated solutions to vary between ± 1 on one of the sides, the cos and sin terms repeat n times on this side, and the function is zero

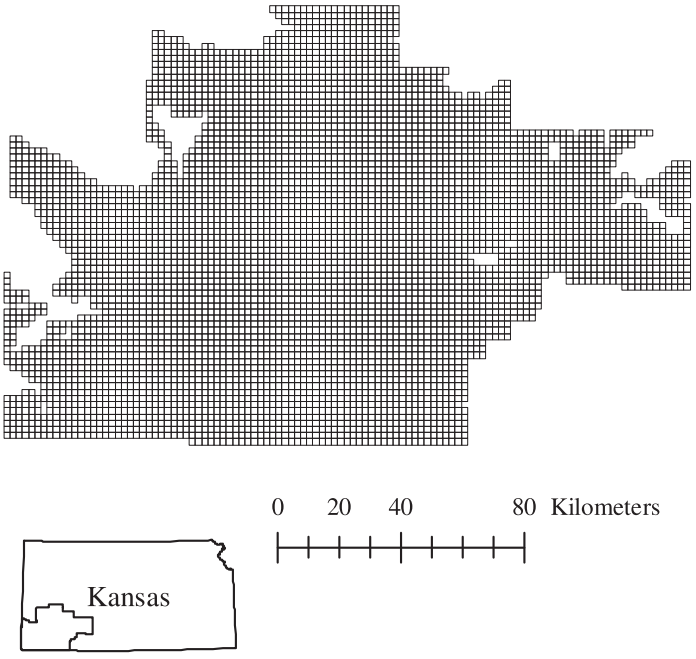

a. Gridded case study domain

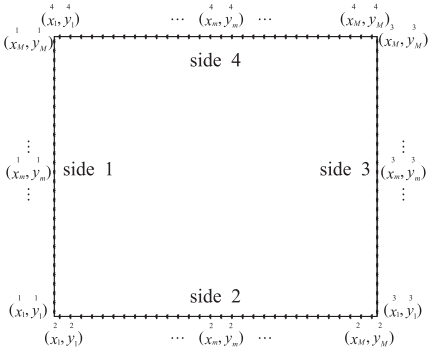

b. Element and its control points

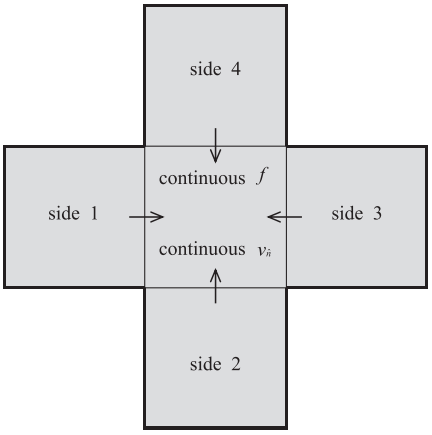

c. Element with adjacent neighbors

Fig. 1. Subdividing a gridded domain into rectangular elements.

on the opposite side. This gives the following set of influence functions

$$
\begin{aligned}
\overset{11}{g}_n &= \frac{\sinh 2\pi n \frac{x_2-x}{y_2-y_1}}{\sinh 2\pi n \frac{x_2-x_1}{y_2-y_1}} \cos 2\pi n \frac{y-y_1}{y_2-y_1} \\
\overset{12}{g}_n &= \frac{\sinh 2\pi n \frac{x_2-x}{y_2-y_1}}{\sinh 2\pi n \frac{x_2-x_1}{y_2-y_1}} \sin 2\pi n \frac{y-y_1}{y_2-y_1} \\
\overset{21}{g}_n &= \cos 2\pi n \frac{x-x_1}{x_2-x_1} \frac{\sinh 2\pi n \frac{y_2-y}{x_2-x_1}}{\sinh 2\pi n \frac{y_2-y_1}{x_2-x_1}} \\
\overset{22}{g}_n &= \sin 2\pi n \frac{x-x_1}{x_2-x_1} \frac{\sinh 2\pi n \frac{y_2-y}{x_2-x_1}}{\sinh 2\pi n \frac{y_2-y_1}{x_2-x_1}} \\
\overset{31}{g}_n &= \frac{\sinh 2\pi n \frac{x-x_1}{y_2-y_1}}{\sinh 2\pi n \frac{x_2-x_1}{y_2-y_1}} \cos 2\pi n \frac{y-y_1}{y_2-y_1} \\
\overset{32}{g}_n &= \frac{\sinh 2\pi n \frac{x-x_1}{y_2-y_1}}{\sinh 2\pi n \frac{x_2-x_1}{y_2-y_1}} \sin 2\pi n \frac{y-y_1}{y_2-y_1} \\
\overset{41}{g}_n &= \cos 2\pi n \frac{x-x_1}{x_2-x_1} \frac{\sinh 2\pi n \frac{y-y_1}{x_2-x_1}}{\sinh 2\pi n \frac{y_2-y_1}{x_2-x_1}} \\
\overset{42}{g}_n &= \sin 2\pi n \frac{x-x_1}{x_2-x_1} \frac{\sinh 2\pi n \frac{y-y_1}{x_2-x_1}}{\sinh 2\pi n \frac{y_2-y_1}{x_2-x_1}}
\end{aligned}
\tag{8}
$$

These functions are written as $\overset{kl}{g}_n(x,y)$, where the first overscript $k = 1,2,3,4$ denotes the four sides, and the second overscript $l = 1,2$ denotes the cosine or sine function respectively.

Solutions to the Laplace equation may also include functional forms with variations not captured by Fourier series alone. A set of influence functions that are constant or vary as a linear or quadratic function of x and y and vary between ± 1 along the boundary of an element are given by

$$
\begin{aligned}
&\overset{0}{g} = 1, \quad \overset{x}{g} = \tfrac{2x-(x_2+x_1)}{x_2-x_1}, \quad \overset{y}{g} = \tfrac{2y-(y_2+y_1)}{y_2-y_1}, \\
&\overset{xy}{g} = \left[\tfrac{2x-(x_2+x_1)}{x_2-x_1}\right]\left[\tfrac{2y-(y_2+y_1)}{y_2-y_1}\right], \\
&\overset{xy2}{g} = \left[\tfrac{2x-(x_2+x_1)}{x_2-x_1}\right]^2 - \left[\tfrac{2y-(y_2+y_1)}{x_2-x_1}\right]^2
\end{aligned}
\tag{9}
$$

These functions provide quadratic variation in the potential along the sides of rectangles and eliminates the Gibb's effect inherent in SOV solutions [32]. Other functions, such as those presented shortly in Eq. (12), may be added to these influence functions to account for additional variations in potential.

2.3. Linear superposition of influence functions

Following the Analytic Element Method, a solution to the Laplace equation over each rectangle is obtained by taking linear combinations of the influence functions

$$
\begin{aligned}
\Phi(\mathbf{c},x,y) = &\overset{0\,0}{c}\overset{0\,0}{g} + \overset{x\,x}{c}\overset{x\,x}{g}(x) + \overset{y\,y}{c}\overset{y\,y}{g}(y) + \overset{xyxy}{c}\overset{xyxy}{g}(x,y) + \overset{xy2xy2}{c}\overset{xy2xy2}{g}(x,y) \\
&+ \sum_{n=1}^{N}\sum_{k=1}^{4}\sum_{l=1}^{2} \overset{kl}{c}_n \overset{kl}{g}_n(x,y) \\
&+ d(x,y)
\end{aligned}
\tag{10}
$$

where the coefficients $\overset{0}{c}, \overset{x}{c}, \overset{y}{c}, \overset{xy}{c}, \overset{xy2}{c}$, and $\overset{kl}{c_n}$ are gathered in the vector

$$\mathbf{c} = \begin{bmatrix} \overset{0}{c} \\ \overset{x}{c} \\ \overset{y}{c} \\ \overset{xy}{c} \\ \overset{xy2}{c} \\ \vdots \\ \overset{kl}{c_n} \\ \vdots \end{bmatrix} \tag{11}$$

Note that n is summed over the N number of times that the Fourier series repeat, k is summed over the number of sides in each rectangle, and l is summed for the cosine and sine functions.

The function d in (10) is used to incorporate other functions in the interior of a rectangle that do not take on the forms of the specified influence functions. For example, our solution in the case study will incorporate wells as point-sinks [45]

$$d = \frac{Q}{2\pi} \ln r \tag{12a}$$

where Q is the strength and r is the radial distance from the sink. Our solution will also incorporate a function with uniform divergence (recharge rate R) across an element, which may be chosen to take different forms but is set here as per [33],

$$\frac{\partial^2 d}{\partial x^2} + \frac{\partial^2 d}{\partial y^2} = -R \quad \rightarrow \quad d = -R\frac{x^2}{2} \tag{12b}$$

and extends the methods to solutions of the Poisson equation. Note that the functions used for d contain only specified parameters (Q and R) to simplify the presentation of solution method to adjust the coefficients $\mathbf{c}$ in (11). Additional functions in d with unknown coefficients, for example line elements placed within rectangles, would require additional complexity to determine those coefficients in the solve algorithms developed next, for example by incorporating the solve matrices for Cauchy integrals presented in [37].

2.4. Solution method to satisfy boundary conditions

While the function Φ in (10) may be evaluated at any point (x, y) in a single element, it is convenient to use matrices to gather the equations used to evaluate Φ at control points where boundary conditions are to be applied. A set of M equally spaced control points on each sides of the element are located at

$$\begin{aligned}
\overset{1}{x}_m &= x_1, \quad \overset{1}{y}_m = y_1 + (y_2 - y_1)\frac{m - \frac{1}{2}}{M} \\
\overset{2}{x}_m &= x_1 + (x_2 - x_1)\frac{m - \frac{1}{2}}{M}, \quad \overset{2}{y}_m = y_1 \\
\overset{3}{x}_m &= x_2, \quad \overset{3}{y}_m = y_1 + (y_2 - y_1)\frac{m - \frac{1}{2}}{M} \\
\overset{4}{x}_m &= x_1 + (x_2 - x_1)\frac{m - \frac{1}{2}}{M}, \quad \overset{4}{y}_m = y_2
\end{aligned} \tag{13}$$

and identified in Fig. 1b.

For a side k with Dirichlet boundary conditions, the potential function at control point m may be specified to be equal to the value of $\overset{k}{\Phi}_m$:

$$\Phi(\mathbf{c}, \overset{k}{x}_m, \overset{k}{y}_m) = \overset{k}{\Phi}_m \quad (m = 1 : M) \tag{14}$$

This gives a set of M equations that may be gathered in the matrices

$$\overset{k}{\mathbf{A}}\,\mathbf{c} = \overset{k}{\mathbf{b}} - \overset{k}{\mathbf{d}} \tag{15}$$

where $\overset{k}{\mathbf{A}}$ contains values obtained by evaluating the influence functions (10) at these points, $\overset{k}{\mathbf{b}}$ contains the specified values $\overset{k}{\Phi}_m$, and $\overset{k}{\mathbf{d}}$ contains values obtained by evaluating the function d at these points:

$$\begin{aligned}
\overset{k}{\mathbf{A}} &= \begin{bmatrix} \vdots & \vdots & \vdots & & \vdots & \\ 1 & \overset{x}{g}(\overset{k}{x}_m) & \overset{y}{g}(\overset{k}{y}_m) & \cdots & \overset{kj}{g}_n(\overset{k}{x}_m, \overset{k}{y}_m) & \cdots \\ \vdots & \vdots & \vdots & & \vdots & \end{bmatrix}, \\
\overset{k}{\mathbf{b}} &= \begin{bmatrix} \vdots \\ \overset{k}{\Phi}_m \\ \vdots \end{bmatrix}, \quad \overset{k}{\mathbf{d}} = \begin{bmatrix} \vdots \\ d\left(\overset{k}{x}_m, \overset{k}{y}_m\right) \\ \vdots \end{bmatrix}
\end{aligned} \tag{16}$$

Likewise, a side with Neumann boundary conditions where the partial derivative in the $\hat{n}$-direction normal to the side is specified at each control point

$$\frac{\partial \Phi\left(\mathbf{c}, \overset{k}{x}_m, \overset{k}{y}_m\right)}{\partial \hat{n}} = -\left(\overset{k}{v}_{\hat{n}}\right)_m \quad (m = 1 : M) \tag{17}$$

may be gathered in the following matrices in (15) that relate the unknown coefficients $\mathbf{c}$ to the Neumann boundary conditions:

$$\begin{aligned}
\overset{k}{\mathbf{A}} &= w\begin{bmatrix} \vdots & \vdots & \vdots & & \vdots & \\ 0 & \frac{\partial \overset{x}{g}}{\partial \hat{n}}(\overset{k}{x}_m) & \frac{\partial \overset{y}{g}}{\partial \hat{n}}(\overset{k}{y}_m) & \cdots & \frac{\partial \overset{kj}{g}_n}{\partial \hat{n}}(\overset{k}{x}_m, \overset{k}{y}_m) & \cdots \\ \vdots & \vdots & \vdots & & \vdots & \end{bmatrix}, \\
\overset{k}{\mathbf{b}} &= w\begin{bmatrix} \vdots \\ -\left(\overset{k}{v}_{\hat{n}}\right)_m \\ \vdots \end{bmatrix}, \quad \overset{k}{\mathbf{d}} = w\begin{bmatrix} \vdots \\ \frac{\partial d}{\partial \hat{n}}(\overset{k}{x}_m, \overset{k}{y}_m) \\ \vdots \end{bmatrix}
\end{aligned} \tag{18}$$

where $\left(\overset{k}{v}_{\hat{n}}\right)_m$ is the normal component of the discharge vector for control point m on side k. The weight w is used to scale these equations to contain terms on the same order as those for Dirichlet conditions (16), and set to $w = (x_2 - x_1)/2\pi N$ in our implementation. Together, the four sides of a rectangle provide a set of $4M$ equations

$$\begin{bmatrix} \overset{1}{\mathbf{A}} \\ \overset{2}{\mathbf{A}} \\ \overset{3}{\mathbf{A}} \\ \overset{4}{\mathbf{A}} \end{bmatrix} \mathbf{c} = \begin{bmatrix} \overset{1}{\mathbf{b}} \\ \overset{2}{\mathbf{b}} \\ \overset{3}{\mathbf{b}} \\ \overset{4}{\mathbf{b}} \end{bmatrix} - \begin{bmatrix} \overset{1}{\mathbf{d}} \\ \overset{2}{\mathbf{d}} \\ \overset{3}{\mathbf{d}} \\ \overset{4}{\mathbf{d}} \end{bmatrix} \tag{19}$$

to solve for the $5 + 8N$ unknown coefficients. The value of N is adjusted to contain enough terms so boundary and continuity conditions are accurately matched and M is chosen so the number of equations is larger than the number of unknowns following the overspecification principle of Janković and Barnes [21]. Note that lower-order number of terms $N = 5$ and $M = 15$ are used in the case study, since the quadratic influence functions control the Gibb's effect and the model accurately matches conditions with a relatively small number of Fourier terms. Higher-order elements with $N = 30$ and $M = 90$ were used for model comparison in the benchmark verification section.

The Analytic Element Method is used to extend the separation of variables solution for a single isolated element in (10) with equations to satisfy boundary conditions in (19) to grids of interconnected elements. Two conditions are specified at control points located along the intersection of the rectangle and the neighboring elements on its four sides (shown in Fig. 1c). The first condition re-

lates the potential at points inside the rectangle to the adjoining elements as follows:

$$\begin{aligned}
&{}^{1}_{k}\alpha\,\Phi({}^{\mathbf{c}}_{\text{rect}}, {}^{1}_{m}x, {}^{1}_{m}y) - {}^{1}_{k}\beta\,\Phi({}^{\mathbf{c}}_{\text{side 1}}, {}^{3}_{m}x, {}^{3}_{m}y) = {}^{1}_{k}\gamma_m \\
&{}^{2}_{k}\alpha\,\Phi({}^{\mathbf{c}}_{\text{rect}}, {}^{2}_{m}x, {}^{2}_{m}y) - {}^{2}_{k}\beta\,\Phi({}^{\mathbf{c}}_{\text{side 2}}, {}^{4}_{m}x, {}^{4}_{m}y) = {}^{2}_{k}\gamma_m \\
&{}^{3}_{k}\alpha\,\Phi({}^{\mathbf{c}}_{\text{rect}}, {}^{3}_{m}x, {}^{3}_{m}y) - {}^{3}_{k}\beta\,\Phi({}^{\mathbf{c}}_{\text{side 3}}, {}^{1}_{m}x, {}^{1}_{m}y) = {}^{3}_{k}\gamma_m \\
&{}^{4}_{k}\alpha\,\Phi({}^{\mathbf{c}}_{\text{rect}}, {}^{4}_{m}x, {}^{4}_{m}y) - {}^{4}_{k}\beta\,\Phi({}^{\mathbf{c}}_{\text{side 4}}, {}^{2}_{m}x, {}^{2}_{m}y) = {}^{4}_{k}\gamma_m \\
&\qquad (m = 1:M)
\end{aligned} \tag{20}$$

where ${}^{k}_{}\alpha, {}^{k}_{}\beta$ and ${}^{k}_{}\gamma_m$ are specified at each control point, and ${}^{\mathbf{c}}_{\text{rect}}$, ${}^{\mathbf{c}}_{\text{side 1}}$, ${}^{\mathbf{c}}_{\text{side 2}}$, ${}^{\mathbf{c}}_{\text{side 3}}$ and ${}^{\mathbf{c}}_{\text{side 4}}$ are the coefficients (11) associated with the rectangle and the side elements. This condition is used to satisfy conservation of energy (continuity of head) across adjacent elements along with the requirement that the head cannot be lower than the base. Implementation of this condition follows [33], by evaluating the potential function in the element with the lowest base elevation (designated with a minus sign), convert this to head using (4), setting the head in the adjacent rectangle to be either this head or the base of the aquifer in this element, and then converting to potential using (1):

$$\begin{aligned}
\Phi^{-}(x,y) &\rightarrow h^{-} \\
h^{-} &\rightarrow h^{+} = \max(B^{+}, h^{-}) \\
h^{+} &\rightarrow \Phi^{+}(x,y)
\end{aligned} \tag{21}$$

This leads to the following coefficients to satisfy the continuity condition in (20)

$$\begin{aligned}
&{}^{1}_{k}\alpha = \frac{1}{{}^{k}_{\text{rect}}}, \quad {}^{1}_{k}\beta = \frac{1}{{}^{k}_{\text{side 1}}}, \quad {}^{1}_{m}\gamma = \frac{\Phi({}^{\mathbf{c}}_{\text{rect}}, {}^{1}_{m}x, {}^{1}_{m}y)}{{}^{k}_{\text{rect}}} - \frac{\Phi({}^{\mathbf{c}}_{\text{side 1}}, {}^{3}_{m}x, {}^{3}_{m}y)}{{}^{k}_{\text{side 1}}} \\
&{}^{2}_{k}\alpha = \frac{1}{{}^{k}_{\text{rect}}}, \quad {}^{2}_{k}\beta = \frac{1}{{}^{k}_{\text{side 2}}}, \quad {}^{2}_{m}\gamma = \frac{\Phi({}^{\mathbf{c}}_{\text{rect}}, {}^{2}_{m}x, {}^{2}_{m}y)}{{}^{k}_{\text{rect}}} - \frac{\Phi({}^{\mathbf{c}}_{\text{side 2}}, {}^{4}_{m}x, {}^{4}_{m}y)}{{}^{k}_{\text{side 2}}} \\
&{}^{3}_{k}\alpha = \frac{1}{{}^{k}_{\text{rect}}}, \quad {}^{3}_{k}\beta = \frac{1}{{}^{k}_{\text{side 3}}}, \quad {}^{3}_{m}\gamma = \frac{\Phi({}^{\mathbf{c}}_{\text{rect}}, {}^{3}_{m}x, {}^{3}_{m}y)}{{}^{k}_{\text{rect}}} - \frac{\Phi({}^{\mathbf{c}}_{\text{side 3}}, {}^{1}_{m}x, {}^{1}_{m}y)}{{}^{k}_{\text{side 3}}} \\
&{}^{4}_{k}\alpha = \frac{1}{{}^{k}_{\text{rect}}}, \quad {}^{4}_{k}\beta = \frac{1}{{}^{k}_{\text{side 4}}}, \quad {}^{4}_{m}\gamma = \frac{\Phi({}^{\mathbf{c}}_{\text{rect}}, {}^{4}_{m}x, {}^{4}_{m}y)}{{}^{k}_{\text{rect}}} - \frac{\Phi({}^{\mathbf{c}}_{\text{side 4}}, {}^{2}_{m}x, {}^{2}_{m}y)}{{}^{k}_{\text{side 4}}}
\end{aligned} \tag{22}$$

Note the coefficient ${}^{k}_{m}\gamma$ must be updated throughout each iterate of the solve process using the strength coefficients from the previous iterate.

The second condition relates the normal component of flux at control points along the four sides of the rectangle to that in the adjacent elements:

$$\begin{aligned}
&{}^{1}_{k}\lambda\,\frac{\partial\Phi({}^{\mathbf{c}}_{\text{rect}}, {}^{1}_{m}x, {}^{1}_{m}y)}{\partial\hat{n}} - {}^{1}_{k}\mu\,\frac{\partial\Phi({}^{\mathbf{c}}_{\text{side 1}}, {}^{3}_{m}x, {}^{3}_{m}y)}{\partial\hat{n}} = {}^{1}_{m}v \\
&{}^{2}_{k}\lambda\,\frac{\partial\Phi({}^{\mathbf{c}}_{\text{rect}}, {}^{2}_{m}x, {}^{2}_{m}y)}{\partial\hat{n}} - {}^{2}_{k}\mu\,\frac{\partial\Phi({}^{\mathbf{c}}_{\text{side 2}}, {}^{4}_{m}x, {}^{4}_{m}y)}{\partial\hat{n}} = {}^{2}_{m}v \\
&{}^{3}_{k}\lambda\,\frac{\partial\Phi({}^{\mathbf{c}}_{\text{rect}}, {}^{3}_{m}x, {}^{3}_{m}y)}{\partial\hat{n}} - {}^{3}_{k}\mu\,\frac{\partial\Phi({}^{\mathbf{c}}_{\text{side 3}}, {}^{1}_{m}x, {}^{1}_{m}y)}{\partial\hat{n}} = {}^{3}_{m}v \\
&{}^{4}_{k}\lambda\,\frac{\partial\Phi({}^{\mathbf{c}}_{\text{rect}}, {}^{4}_{m}x, {}^{4}_{m}y)}{\partial\hat{n}} - {}^{4}_{k}\mu\,\frac{\partial\Phi({}^{\mathbf{c}}_{\text{side 4}}, {}^{2}_{m}x, {}^{2}_{m}y)}{\partial\hat{n}} = {}^{4}_{m}v \\
&\qquad (m = 1:M)
\end{aligned} \tag{23}$$

This condition is used to satisfy conservation of mass (continuity of flow) where the normal component of the discharge per width is continuous across adjacent elements

$$Q^{-}_{\hat{n}} = Q^{+}_{\hat{n}} \tag{24}$$

This is satisfied by setting ${}^{k}_{}\lambda = 1, {}^{k}_{}\mu = 1$ and ${}^{k}_{m}v = 0$ in (23), although other conditions might be envisioned where the derivative in the normal direction jumps across adjacent elements. Likewise, other applications might utilize a continuous potential across adjacent elements obtained by setting ${}^{k}_{}\alpha = 1, {}^{k}_{}\beta = 1$, and ${}^{k}_{m}\gamma = 0$. Note that since overspecification is applied, conservation of mass is satisfied across control points in a least square sense. The errors associated with this approximation are quantified later in the benchmark verification.

A system of equations is developed next to solve for the unknown coefficients associated with the rectangle and its four adjacent neighbors shown in Fig. 1c. This partitioning of elements was chosen as it gathers those elements necessary to satisfy continuity conditions across all sides of a rectangle into as small a set as possible to achieve the fastest possible computational time. Dirichlet conditions are specified along the outer boundary of this group of elements, and the continuity conditions are applied across the interface of adjacent elements. The equations that relate the strengths of the five rectangles to the set of boundary conditions imposed on the rectangle attached to side 1 is given by

$$\begin{bmatrix}
0 & {}^{1}_{\text{side 1}}\mathbf{A} & 0 & 0 & 0 \\
0 & {}^{2}_{\text{side 1}}\mathbf{A} & 0 & 0 & 0 \\
{}^{1}_{\text{rect}}\alpha\,{}^{1}_{}\mathbf{A} & -{}^{1}_{\text{side 1}}\beta\,{}^{3}_{}\mathbf{A} & 0 & 0 & 0 \\
0 & {}^{4}_{\text{side 1}}\mathbf{A} & 0 & 0 & 0
\end{bmatrix}
\begin{bmatrix}
{}^{\mathbf{c}}_{\text{rect}} \\ {}^{\mathbf{c}}_{\text{side 1}} \\ {}^{\mathbf{c}}_{\text{side 2}} \\ {}^{\mathbf{c}}_{\text{side 3}} \\ {}^{\mathbf{c}}_{\text{side 4}}
\end{bmatrix}
=
\begin{bmatrix}
{}^{1}_{\text{side 1}}\mathbf{b} \\ {}^{2}_{\text{side 1}}\mathbf{b} \\ {}^{1}_{\text{rect}}\alpha\,{}^{1}_{}\mathbf{b} - {}^{1}_{\text{side 1}}\beta\,{}^{3}_{}\mathbf{b} \\ {}^{4}_{\text{side 1}}\mathbf{b}
\end{bmatrix}
-
\begin{bmatrix}
{}^{1}_{\text{side 1}}\mathbf{d} \\ {}^{2}_{\text{side 1}}\mathbf{d} \\ {}^{1}_{\text{rect}}\alpha\,{}^{1}_{}\mathbf{d} - {}^{1}_{\text{side 1}}\beta\,{}^{3}_{}\mathbf{d} \\ {}^{4}_{\text{side 1}}\mathbf{d}
\end{bmatrix} \tag{25a}$$

Here, the Dirichlet condition along the three sides of this rectangle that do not adjoin side 1 of the central rectangle are contained in the matrices ${}^{1}_{\text{side 1}}\mathbf{A}$, ${}^{2}_{\text{side 1}}\mathbf{A}$ and ${}^{4}_{\text{side 1}}\mathbf{A}$; ${}^{1}_{\text{side 1}}\mathbf{b}$, ${}^{2}_{\text{side 1}}\mathbf{b}$, and ${}^{4}_{\text{side 1}}\mathbf{b}$ are filled using (16); and ${}^{1}_{\text{side 1}}\mathbf{d}$, ${}^{2}_{\text{side 1}}\mathbf{d}$ and ${}^{4}_{\text{side 1}}\mathbf{d}$ take on the value of the interior function for the rectangle adjacent to side 1. The continuity condition for side 1 in (20) is satisfied by filling ${}^{1}_{\text{rect}}\mathbf{A}$, ${}^{1}_{\text{rect}}\mathbf{b}$ and ${}^{1}_{\text{rect}}\mathbf{d}$ with values associated with the rectangle on side 1; and filling ${}^{3}_{\text{side 1}}\mathbf{A}$, ${}^{3}_{\text{side 1}}\mathbf{b}$ and ${}^{3}_{\text{side 1}}\mathbf{d}$ with the contributions for the adjacent rectangle. Note that the these matrices for **A** and **d** are fixed, but the matrix **b** must be updated as iteration progresses. Similar equations exist for side 2

$$\begin{bmatrix}
0 & 0 & {}^{1}_{\text{side 2}}\mathbf{A} & 0 & 0 \\
0 & 0 & {}^{2}_{\text{side 2}}\mathbf{A} & 0 & 0 \\
0 & 0 & {}^{3}_{\text{side 2}}\mathbf{A} & 0 & 0 \\
{}^{2}_{\text{rect}}\alpha\,{}^{2}_{}\mathbf{A} & 0 & -{}^{2}_{\text{side 2}}\beta\,{}^{4}_{}\mathbf{A} & 0 & 0
\end{bmatrix}
\begin{bmatrix}
{}^{\mathbf{c}}_{\text{rect}} \\ {}^{\mathbf{c}}_{\text{side 1}} \\ {}^{\mathbf{c}}_{\text{side 2}} \\ {}^{\mathbf{c}}_{\text{side 3}} \\ {}^{\mathbf{c}}_{\text{side 4}}
\end{bmatrix}
=
\begin{bmatrix}
{}^{1}_{\text{side 2}}\mathbf{b} \\ {}^{2}_{\text{side 2}}\mathbf{b} \\ {}^{3}_{\text{side 2}}\mathbf{b} \\ {}^{2}_{\text{rect}}\alpha\,{}^{2}_{}\mathbf{b} - {}^{2}_{\text{side 2}}\beta\,{}^{4}_{}\mathbf{b}
\end{bmatrix}
-
\begin{bmatrix}
{}^{1}_{\text{side 2}}\mathbf{d} \\ {}^{2}_{\text{side 2}}\mathbf{d} \\ {}^{3}_{\text{side 2}}\mathbf{d} \\ {}^{2}_{\text{rect}}\alpha\,{}^{2}_{}\mathbf{d} - {}^{2}_{\text{side 2}}\beta\,{}^{4}_{}\mathbf{d}
\end{bmatrix} \tag{25b}$$

for side 3

$$\begin{bmatrix}
{}^{3}_{\text{rect}}\alpha\,{}^{3}_{}\mathbf{A} & 0 & 0 & -{}^{3}_{\text{side 3}}\beta\,{}^{1}_{}\mathbf{A} & 0 \\
0 & 0 & 0 & {}^{2}_{\text{side 3}}\mathbf{A} & 0 \\
0 & 0 & 0 & {}^{3}_{\text{side 3}}\mathbf{A} & 0 \\
0 & 0 & 0 & {}^{4}_{\text{side 3}}\mathbf{A} & 0
\end{bmatrix}
\begin{bmatrix}
{}^{\mathbf{c}}_{\text{rect}} \\ {}^{\mathbf{c}}_{\text{side 1}} \\ {}^{\mathbf{c}}_{\text{side 2}} \\ {}^{\mathbf{c}}_{\text{side 3}} \\ {}^{\mathbf{c}}_{\text{side 4}}
\end{bmatrix}
=
\begin{bmatrix}
{}^{3}_{\text{rect}}\alpha\,{}^{3}_{}\mathbf{b} - {}^{3}_{\text{side 3}}\beta\,{}^{1}_{}\mathbf{b} \\ {}^{2}_{\text{side 3}}\mathbf{b} \\ {}^{3}_{\text{side 3}}\mathbf{b} \\ {}^{4}_{\text{side 3}}\mathbf{b}
\end{bmatrix}
-
\begin{bmatrix}
{}^{3}_{\text{rect}}\alpha\,{}^{3}_{}\mathbf{d} - {}^{3}_{\text{side 3}}\beta\,{}^{1}_{}\mathbf{d} \\ {}^{2}_{\text{side 3}}\mathbf{d} \\ {}^{3}_{\text{side 3}}\mathbf{d} \\ {}^{4}_{\text{side 3}}\mathbf{d}
\end{bmatrix} \tag{25c}$$

and for side 4

$$\begin{bmatrix} 0 & 0\,0\,0 & \overset{1}{\underset{\text{side 4}}{\mathbf{A}}} \\ \alpha\,\overset{4}{\underset{\text{rect}}{\mathbf{A}}} & 0\,0\,0 & -\beta\,\overset{2}{\underset{\text{side 4}}{\mathbf{A}}} \\ 0 & 0\,0\,0 & \overset{3}{\underset{\text{side 4}}{\mathbf{A}}} \\ 0 & 0\,0\,0 & \overset{4}{\underset{\text{side 4}}{\mathbf{A}}} \end{bmatrix} \begin{bmatrix} \underset{\text{rect}}{\mathbf{c}} \\ \underset{\text{side 1}}{\mathbf{c}} \\ \underset{\text{side 2}}{\mathbf{c}} \\ \underset{\text{side 3}}{\mathbf{c}} \\ \underset{\text{side 4}}{\mathbf{c}} \end{bmatrix} = \begin{bmatrix} \overset{1}{\underset{\text{side 4}}{\mathbf{b}}} \\ \alpha\,\overset{4}{\underset{\text{rect}}{\mathbf{b}}} - \beta\,\overset{2}{\underset{\text{side 4}}{\mathbf{b}}} \\ \overset{3}{\underset{\text{side 4}}{\mathbf{b}}} \\ \overset{4}{\underset{\text{side 4}}{\mathbf{b}}} \end{bmatrix} - \begin{bmatrix} \overset{1}{\underset{\text{side 4}}{\mathbf{d}}} \\ \alpha\,\overset{4}{\underset{\text{rect}}{\mathbf{d}}} - \beta\,\overset{2}{\underset{\text{side 4}}{\mathbf{d}}} \\ \overset{3}{\underset{\text{side 4}}{\mathbf{d}}} \\ \overset{4}{\underset{\text{side 4}}{\mathbf{d}}} \end{bmatrix} \tag{25d}$$

The conditions associated with continuity of the derivative in the normal direction (23) for the groundwater application may be gathered in the following matrices

$$\begin{bmatrix} \overset{1}{\underset{\text{rect}}{\mathbf{A}}} & -\overset{3}{\underset{\text{side 1}}{\mathbf{A}}} & 0 & 0 & 0 \\ \overset{2}{\underset{\text{rect}}{\mathbf{A}}} & 0 & -\overset{4}{\underset{\text{side 2}}{\mathbf{A}}} & 0 & 0 \\ \overset{3}{\underset{\text{rect}}{\mathbf{A}}} & 0 & 0 & -\overset{1}{\underset{\text{side 3}}{\mathbf{A}}} & 0 \\ \overset{4}{\underset{\text{rect}}{\mathbf{A}}} & 0 & 0 & 0 & -\overset{2}{\underset{\text{side 4}}{\mathbf{A}}} \end{bmatrix} \begin{bmatrix} \underset{\text{rect}}{\mathbf{c}} \\ \underset{\text{side 1}}{\mathbf{c}} \\ \underset{\text{side 2}}{\mathbf{c}} \\ \underset{\text{side 3}}{\mathbf{c}} \\ \underset{\text{side 4}}{\mathbf{c}} \end{bmatrix} = \begin{bmatrix} 0 \\ 0 \\ 0 \\ 0 \end{bmatrix} - \begin{bmatrix} \overset{1}{\mathbf{d}} \\ \overset{2}{\mathbf{d}} \\ \overset{3}{\mathbf{d}} \\ \overset{4}{\mathbf{d}} \end{bmatrix} \tag{26}$$

where the rectangle's matrices $\overset{1}{\underset{\text{rect}}{\mathbf{A}}}$, $\overset{2}{\underset{\text{rect}}{\mathbf{A}}}$, $\overset{3}{\underset{\text{rect}}{\mathbf{A}}}$ and $\overset{4}{\underset{\text{rect}}{\mathbf{A}}}$ are filled with values associated with the normal component of the vector field using (18); and the matrices $\overset{1}{\underset{\text{side 1}}{\mathbf{A}}}$, $\overset{2}{\underset{\text{side 2}}{\mathbf{A}}}$, $\overset{3}{\underset{\text{side 3}}{\mathbf{A}}}$ and $\overset{4}{\underset{\text{side 4}}{\mathbf{A}}}$ contain the contributions to the normal component of the vector field for the adjacent rectangles. Continuity also requires that the interior vectors in this equation: $\overset{1}{\mathbf{d}}$, $\overset{2}{\mathbf{d}}$, $\overset{3}{\mathbf{d}}$ and $\overset{4}{\mathbf{d}}$ contain derivatives of the interior function d for the rectangle (18) minus this derivative for the functions interior to the adjacent rectangle on the side associated with $\overset{k}{\mathbf{d}}$.

The system of equations in (25) and (26) contains $5(4M)$ equations and $5(5+8N)$ unknowns associated with the rectangle and its neighbors in Fig. 1c. These matrices are easily adapted for rectangles with boundaries that contain both the edge of the model domain (with Dirichlet or Neumann conditions) and adjacent elements (with continuity conditions) by removing the equations and strengths associated with the side (s), and replacing those conditions with the corresponding portion of the matrices for Dirichlet (16) or Neumann (18) conditions. We adopted an iterative solution method [21] to achieve a solution across all rectangles that cycles through all rectangles and updates coefficients for each rectangle while holding the strengths of the other rectangles at the value of the previous iterate. Upon completion of each iterate, the value of the potential is computed at the control points of each rectangle as it is needed in the side element portions of (25) for the next iterate. Iteration continuous until only small changes occur between successive iterates (maximum difference in head at control points between successive iterates of 10^{-6}m in the benchmark studies). This schema allows for parallelization and was implemented in Scilab and executed on Beocat, the Beowulf grid computing cluster at Kansas State University.

3. Benchmark model verification

While the influence functions for rectangular elements obtained using separation of variables exactly satisfy the governing equations (to within computer accuracy), errors exist in approximating boundary conditions using the Analytic Element Method. Two benchmark comparisons were conducted to verify the capacity of the model to accurately reproduce continuity and boundary conditions. The first examines the distribution of head between adjacent rectangles when a high capacity well (singularity) exists in one rectangle near their common boundary. The second examines discharge across rectangular elements in a heterogeneous porous media.

3.1. Conservation of energy (continuity of head)

A benchmark solution is shown in the top row of Fig. 2 for a domain with fixed heads to the left ($x = x_1$) and right ($x = x_2$), and impermeable conditions on the bottom ($y = y_1$) and top ($y = y_2$). The particular configuration is shown for rectangular dimensions x_1=-8 m, x_2=8 m, y_1=-4 m and y_2=4 m; aquifer parameters B = 0, H = 1 m and k = 10 m/day; boundary conditions $h(x_1)$=10 m and $h(x_2)$=9.984 m; and the head is shown at 32 contours with intervals of Δh=0.0005 m. The well is located at $z_w = x_w + iy_w$ with x_w=-0.1 m, $y_w = 0$, and pumping rate Q. This solution was obtained using the complex potential obtained from the method of images:

$$\begin{aligned} \Omega &= \Phi + i\Psi \\ &= \frac{Q}{2\pi}\ln(z - z_w) + Q_{x0}x + \Phi_0 + \sum_{i=1}^{N_x}\sum_{j=1}^{4}\sum_{k=1}^{N_y}\sum_{l=1}^{4}(-1)^j \frac{Q}{2\pi}\ln[z \\ &\quad - (x_{ij} + iy_{kl})] \end{aligned} \tag{27}$$

where the image wells are located by reflection across the lower and upper bounds of the domain:

$$\begin{aligned} x_{i1} &= x_1 - 2(i-1)(x_2 - x_1) - (x_w - x_1) \\ x_{i2} &= x_1 - 2i(x_2 - x_1) + (x_w - x_1) \\ x_{i3} &= x_1 + 2i(x_2 - x_1) - (x_w - x_1) \\ x_{i4} &= x_1 + 2i(x_2 - x_1) + (x_w - x_1) \\ y_{k1} &= y_1 - 2(k-1)(y_2 - y_1) - (y_w - y_1) \\ y_{k2} &= y_1 - 2k(y_2 - y_1) + (y_w - y_1) \\ y_{k3} &= y_1 + 2k(y_2 - y_1) - (y_w - y_1) \\ y_{k4} &= y_1 + 2k(y_2 - y_1) + (y_w - y_1) \end{aligned} \tag{28}$$

Note that the $(-1)^j$ term sets the sign of the image wells to reproduce the specified boundary conditions. The values of Q_{x0} and Φ_0 are set such that $\Phi(x = x_1) = \Phi_1$ and $\Phi(x = x_2) = \Phi_2$, where these potentials are obtained from h_1 and h_2 using (1). The number of images was chosen such that $N_x = N_y = 20$, which satisfied the boundary conditions at the left and right to within $0.002\Delta h$. Streamlines with constant Ψ illustrate that the capture zone for the well contains approximately 1/2 the discharge flowing from the left to right boundary.

This method of images solution is compared to that obtained using rectangular elements in Fig. 2. The second row shows two lower-order rectangles (number of strength coefficients, $N = 5$), where a well was added to the interior function d in (10) for the rectangle to the left of x = 0 but not included in the right rectangle. The graphs in the right column shows head at the intersection of the two rectangles ($x = 0$ and y between y_1 and y_2) with intervals of 1 dimensionless unit representing a change in head of Δh, the contour interval spacing. Results illustrate that, while this lower-order solution matches continuity conditions of head being equal in both rectangles at control points fairly well, there is a consistent error with head being too low when compared to the exact solution (by a factor of $2\Delta h$). Using the rectangles with higher-order elements (N = 30) in the third row of Fig. 2 gives a more accurate solution, with a maximum absolute difference between this and the exact solutions of $0.06\Delta h$ and an average difference of $0.002\Delta h$ (the same accuracy with which the method of images matches boundary conditions to the left and right). Another method to increase the accuracy of the solution is presented in the last row, where lower-order rectangles (N = 5) were used but the well

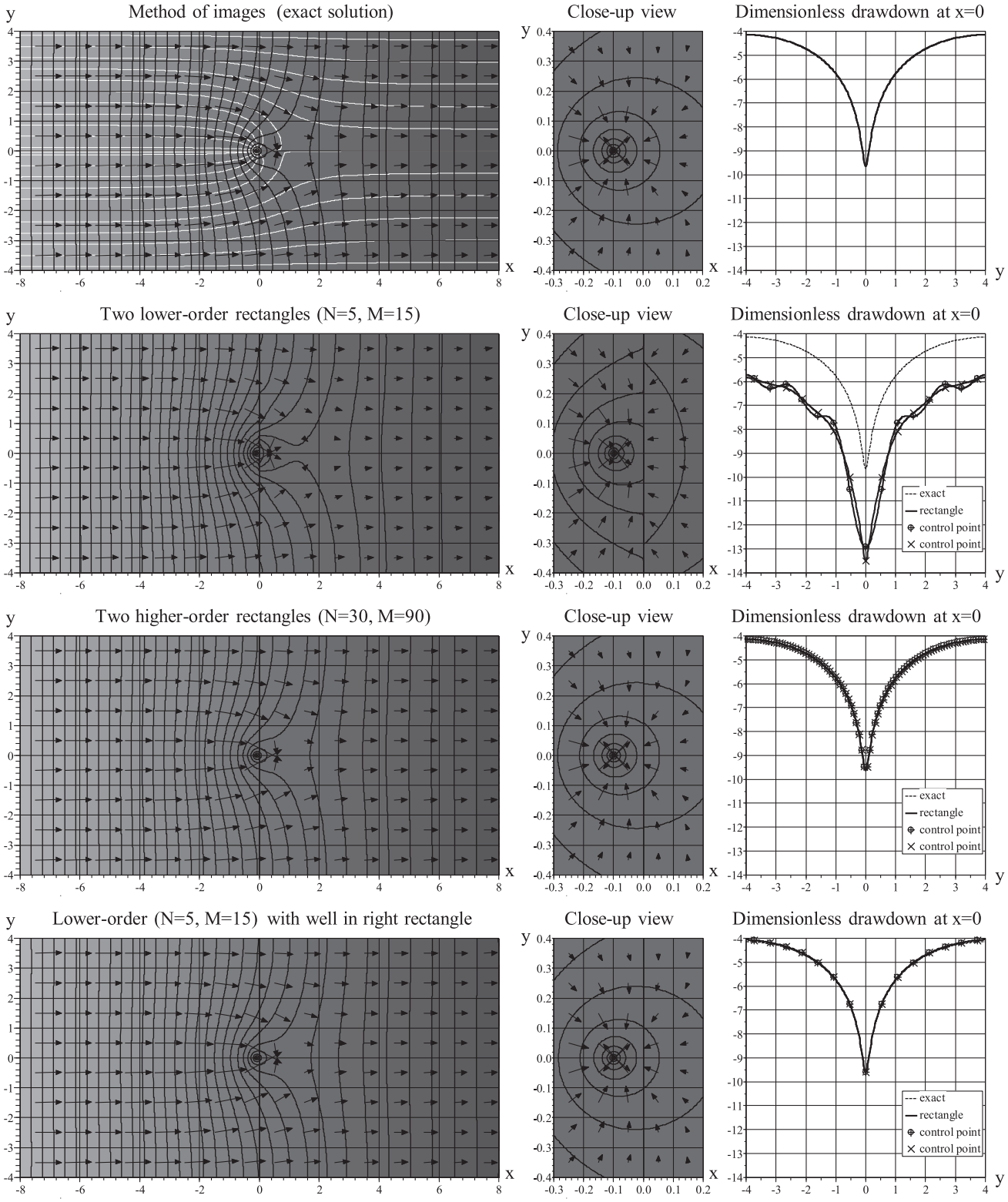

Fig. 2. Benchmark for conservation of energy: comparing rectangular elements near a singularity to the method of images (exact solution). The domain has fixed heads on the left and right sides, and no flow occurs across the top and bottom sides.

was also included in d in (10) for the right rectangle, thereby reproducing the functional variation of the singularity directly in the equation for this rectangle. The maximum absolute difference between this and the exact solutions is $0.10\Delta h$ and the average difference is $0.04\Delta h$.

Thus, our AEM solution accurately satisfies the condition of conservation of energy across adjacent rectangles, with greater precision obtained by increasing the number of coefficients or by adding interior functions to account for the singular behavior occurring outside a rectangle.

3.2. Conservation of mass (continuity of flow)

The benchmark solution containing rectangle elements that completely fill a heterogeneous porous media, each with distinct properties as illustrated in Fig. 3. The hydraulic conductivity is log normally distributed

$$k = k_G e^Y, \quad \mu_Y = 0, \quad \sigma_Y = 1.5 \tag{29}$$

where k_G is the geometric mean, and μ_Y and σ_Y are the mean and standard deviation of Y [14]. The particular configuration shown in Fig. 3 contains 16 lower-order ($N = 5$) rectangles with aquifer parameters $B = 1$ m, $H = 1$ m and k_G=10 m/day, impermeable boundary conditions at the bottom and top, boundary conditions of fixed head at the left ($h = 10$ m) and right ($h = 9$ m), and the head is shown at 50 contours with intervals of Δh=0.02 m. The standard deviation σ_y=1.5 was chosen such that the porous media is highly

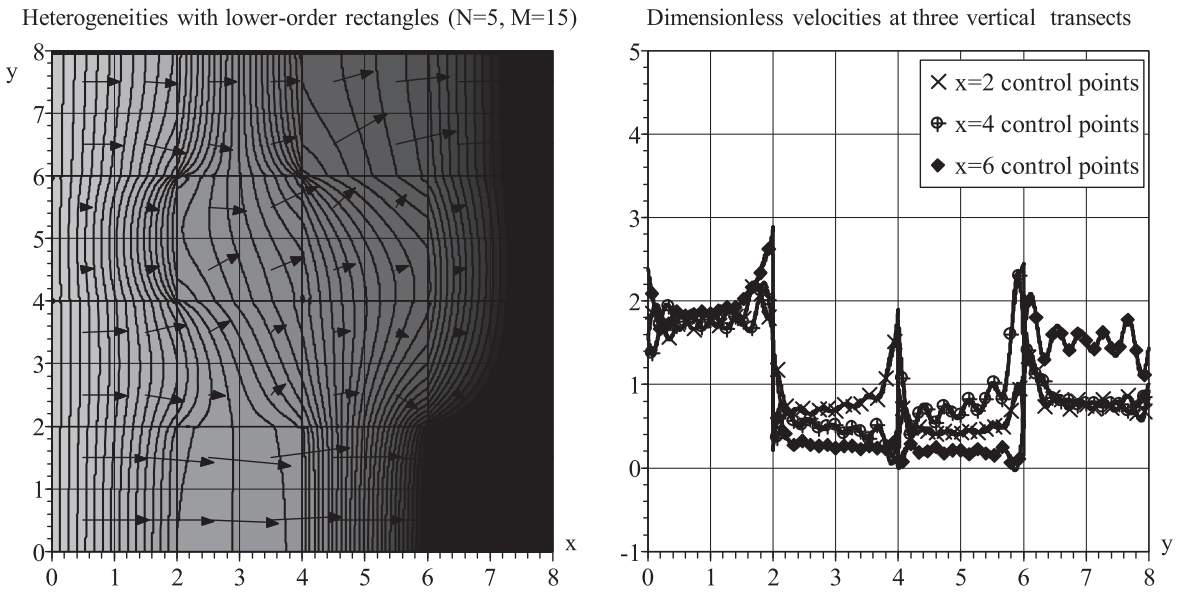

Fig. 3. Benchmark for conservation of mass: comparing the discharge per width across transects in a heterogeneous media. The head is uniform along the left and right sides, no flow occurs across the top and bottom sides, and the log normally distributed hydraulic conductivity jumps across adjacent rectangles.

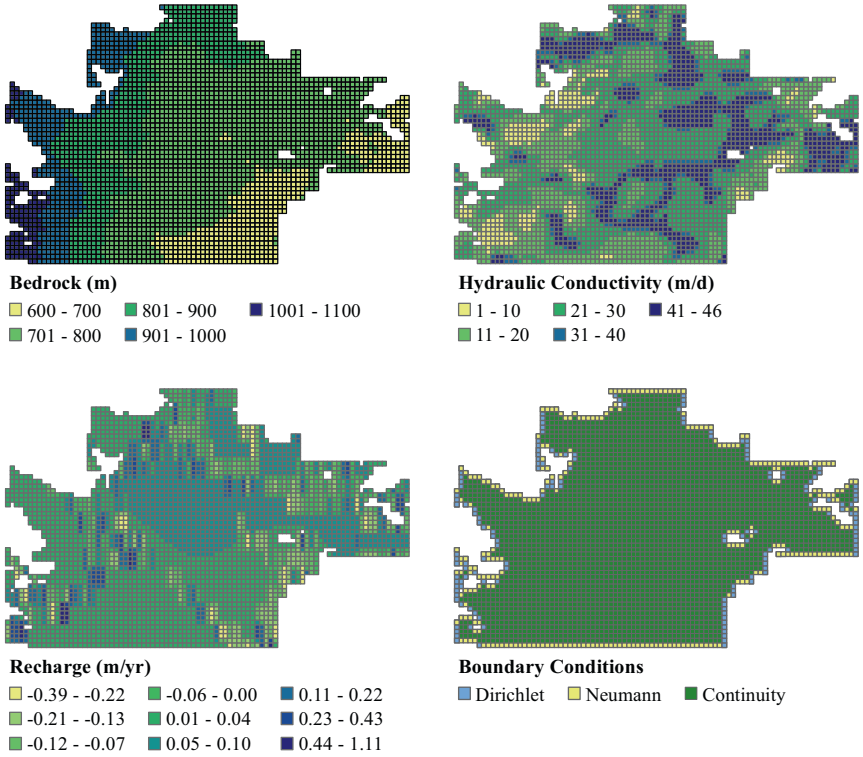

Fig. 4. Data for the groundwater case study.

heterogeneous, and yet each rectangle has a value of k that allows easily discernible variation in head contours to visually verify conservation of energy. There is no correlation between the conductivities of the rectangles, following [23].

This solution was used to plot the normal component of the discharge per width (Q_x) across adjacent rectangles in the right graph of Fig. 3. This is shown along the boundaries of rectangles on both sides of three transects where $x = 2$, 4 and 6 m, and y varies between the bottom ($y = 0$ m) and top ($y = 8$ m) of the domain. The discharge per width is plotted on a dimensionless axis obtained by dividing Q_x by the average discharge that enters the domain on the left and leaves the domain on the right. Results illustrate that the normal component of flow between points on each side of the three interfaces are very close, with an average absolute difference between all control points for all transects of 0.024, or about 1/10 the distance between tick marks on the y-axis. The net flux across the domain was also computed across the three transects by numerical integration of the normal component of flow, and these dimensionless discharges match to within 0.0009. This means that less that 0.09% of the net discharge is numerically lost or gained as flow moves across the rectangles in the domain.

Thus, our AEM solution accurately satisfies the condition of conservation of mass for the discharge vector at individual points in neighboring rectangles, and for the net discharge occurring across adjacent rectangles. Note that head contours in both Fig. 2 and 3 illustrate that boundary conditions are accurately satisfied for the constant head at the left and right, and for the no flow conditions at the bottom and top (perpendicular to contours of constant head).

4. Case study and results

The capacity of our AEM approach to model practical problems is illustrated by this case study of groundwater pumping in the High Plains Aquifer of southwest Kansas, identified in Fig. 1a. Groundwater use for irrigated agriculture supports a dynamic regional economy [3,36] and this congressional district has the highest market value for agricultural production in the United States [46]. The region is experiencing sustainability challenges associated with a declining resource where groundwater is being tapped beyond the rate of natural recharge [39]. Addressing this problem requires a computational method, such as our AEM model, that is broad in scope and capable of modeling a large region while also incorporating the local detail of drawdown from wells [35].

The data for the study region are illustrated in Fig. 4. The base elevation and hydraulic conductivity were obtained from contour maps developed for the USGS Regional Aquifer-System Analysis project [18] and digitized by [9,10]. This model incorporates surface water interactions associated with both recharge and the gaining and losing sections of rivers [2], using the rate of recharge obtained from contour maps of terrestrial recharge developed for the Kansas Division of Water Resources [20] and subtracting the

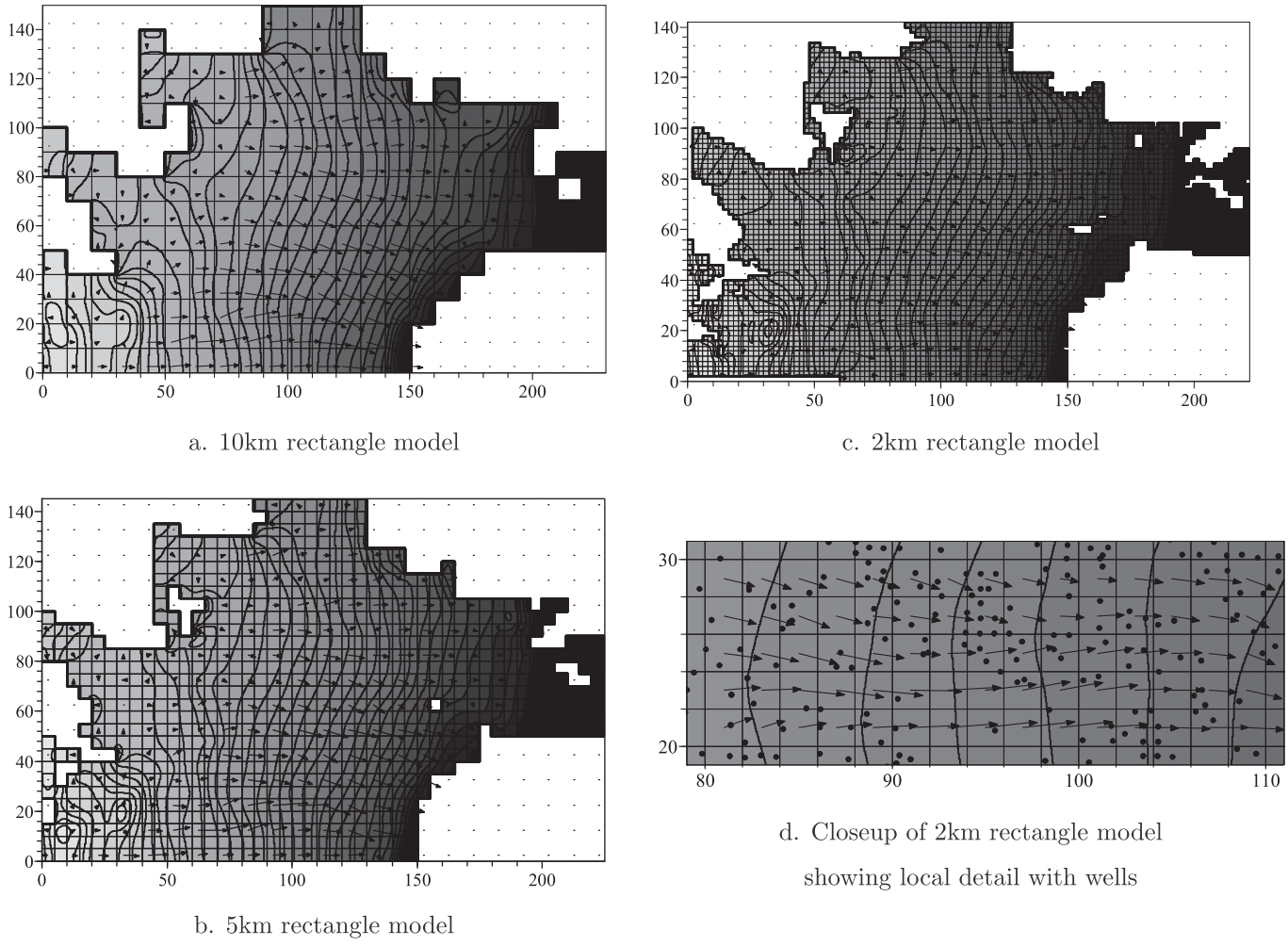

Fig. 5. The groundwater model results for the High Plains Aquifer in southwestern Kansas, showing rectangular elements, head contours at intervals of 10 m, and domain dimensions specified in units of km. Results are shown for square elements with sides of length 10 km, 5 km and 2 km, and a closeup view is shown for the 2 km model with wells.

Table 1
The computational costs associated with solving the system of equations and then gridding the head for the High Plains groundwater model. Results illustrate that the solve time necessary to determine coefficients scales with the number of rectangles and the number of iterates. The grid time to compute the head across 500 × 500 points is approximately the same time as one solve iteration. The computer memory storage requirements for all data including solve matrices for all rectangles is also reported. The number of coefficients was set to $N = 3$ for the 2 km model due to memory storage limitations.

Rectangle size	10 km			5 km			2 km		
Convergence criteria [m]	10^{-4}	10^{-5}	10^{-6}	10^{-4}	10^{-5}	10^{-6}	10^{-4}	10^{-5}	10^{-6}
Solve time (t_S) [hr]	2.08	2.54	3.04	26.53	33.54	39.38	315.05	474.75	602.52
# of iterations (I)	707	888	1069	2186	2832	3478	6920	9496	12073
# of rectangles (J)	224	224	224	859	859	859	5096	5096	5096
Solve per iterate (t_S/IJ) [sec]	0.047	0.046	0.046	0.051	0.050	0.047	0.032	0.035	0.035
Grid time (t_G) [sec]	12	13	13	42	48	51	196	197	192
Grid per rectangle (t_G/J) [sec]	0.054	0.058	0.058	0.049	0.056	0.059	0.038	0.039	0.038
Memory [MB]		111			440			1763	
Solve coefficients		$N = 5$, $M = 15$			$N = 5$, $M = 15$			$N = 3$, $M = 15$	

rate of baseflow extraction occurring from groundwater to surface water [4]. Note that this results in some negative values for recharge, indicating net extraction of groundwater to surface water exceeding terrestrial recharge over the rectangle. Raster maps were obtained for these data using the "Topo to Raster" tool in ArcGIS and results were aggregated to the size of the rectangles, and these properties were assumed uniform in each element. Wells were incorporated in some of the elements using pumping rates and locations obtained from the WRIS (Water Rights Information System) database at the Kansas Division of Water Resources.

Boundary and continuity conditions were specified as follows. Dirichlet conditions along the western and eastern boundaries were obtained using the head from predevelopment maps of groundwater elevation [11,18]. The location of these boundaries was identified by limiting the model domain to rectangles with a predevelopment saturated thickness of at least 5 m following [27], a criteria that was also applied to identify rectangles inside the domain where groundwater did not exist. Neumann conditions along the northern and southern boundaries specify a normal component $Q_{\hat{n}} = 0$, as groundwater flow in the region is predominated by a west-to-east sloping bedrock [39]. Continuity conditions were applied across adjacent rectangles to satisfy conservation of energy and mass conditions.

The model was executed using elements with sides of length 10, 5 and 2 km, and the resulting distribution of head is illustrated in Fig. 5, where x and y units are km and head is contoured at 10 m intervals. The local view in Fig. 5d illustrates the capacity of this model to incorporate local detail of well-on-well interactions within a regional setting. Each well individually withdraws a much lower percentage of the regional flow than the benchmark study in Fig. 2, and hence, drawdown is not as pronounced as in that figure. The solution accurately matches boundary and continuity conditions, and show the gentle west to east head gradient that extends existing stepping base models [33,38] to a two-dimensional setting.

The computational costs associated with the case study model are reported in Table 1. For each grid resolution, the model was run until the error (maximum difference in head between successive iterates across all control points for all rectangles) was 10^{-4}, 10^{-5} or 10^{-6}, and the number of iterates required to achieve this accuracy are reported. The time to solve scales directly with the number of iterates and the number of rectangle elements in the domain. The time to evaluate the solution by gridding head across is relatively small, and on the same order as one solve iteration. Memory requirements scale with the number of rectangles, as the solve matrices were saved individually for each rectangle in our implementation. Considerable computational advantages would be realized through modifying code to use parallel processing of the iterative solve process [6].

5. Conclusions and discussion

A new model is developed by adapting the Analytic Element Method to extend separation of variables solutions to rectangular gridded domains. First a domain is discretized as a set of interconnected rectangular elements in Fig. 1, each with unique properties associated with the problem domain (Fig. 4). A set of influence functions are developed from separation of variables (8) along with constant, linear and quadratic functions (9) that help resolve the Gibbs phenomenon. These functions are linearly superimposed with functions for wells and recharge to give the potential function for a rectangle (10). Equations are developed to satisfy boundary conditions at control points - Fig. 1 - and gathered in matrices - (15) and (19) - for Dirichlet (16) and Neumann (18) conditions. Continuity conditions are developed for the potential (25) and the normal component of its derivative (26) to satisfy conservation laws across adjacent rectangles. This system of equations is solved iteratively to obtain a continuously varying function across a rectangular grid with specified boundary and continuity conditions.

Benchmark studies were performed to verify that the model accurately satisfies continuity and boundary conditions. The first benchmark compared the solution to that obtained via the method of images for a high capacity well in a bounded domain, and results in Fig. 3 illustrate that conservation of energy is accurately satisfied. The second benchmark studied rectangles with log normal heterogeneity in hydraulic conductivity, and results in Fig. 3 illustrate that conservation of mass is accurately satisfied. A case study illustrates the capabilities of the AEM approach to model groundwater in the High Plains Aquifer of southwestern Kansas, identified in Fig. 1. This region is spatially large with variable aquifer and hydrologic properties, and local interactions amongst irrigation wells. A variety of GIS vector and raster data sources were used to develop unique properties for each rectangular element in Fig. 4. Results in Fig. 5 illustrate that boundary and continuity conditions are accurately matched, and that the model generates a continuous function across the region that incorporates the detail of local well pumping. Table 1 summarizes the impact of changes in resolution on computational costs associated with running the model.

Our new model for rectangular gridded domains poses several advantages. Unlike the Embedded Matrix Method that places heterogeneities inside a homogeneous background [15], rectangular heterogeneities may completely fill the domain (see Fig. 3). Such elements allow for jumps in properties such as hydraulic conductivity and aquifer bedrock across a study area (see Fig. 5). Computing head and velocity at grid points in a domain with rectangular elements only requires evaluation of the influence functions and interior functions for the rectangle in which the evaluation point resides, (10), resulting in evaluation time as documented in Table 1,

which are much faster than previous studies of the region that used Cauchy integrals [38]. Our model ties the rectangular elements directly to the raster data sources in ArcGIS (see Fig. 4), which were obtained through spatial analysis of the underlying data sets, with the vector datasets for the location and pumping rates for wells, which retain their point data attributes. The size of the elements for the regional model – 2.5, 5 and 10 km in Fig. 5 – are on the same order as previous finite difference models – with grid spacings of between 1.61–16.1 km [18,27] – and provide a continuously varying function within rectangles across the region that accurately captures well-on-well interactions. The capabilities of the methods to accurately reproduce the singular behavior of well drawdown near the side of a rectangle was established in Fig. 3.

Future work is envisioned to extend the existing model that was executed on a grid computing system. By isolating evaluation of functions to those occurring within isolated rectangles, the computations associated with head and velocity as well as the iterative solve process are well suited for parallel computations. The mathematical and numerical implementation is applicable to other fields of study with interconnected rectangular elements, such as heat conduction, electrical conduction and unsaturated groundwater flow.

Acknowledgments

The reviews by Prof. Henk Haitjema, Dr. Ed Veling and three anonymous reviewers provided great insight toward clarifying and strengthening the presentation of findings and were most appreciated. The authors gratefully acknowledge financial support from the National Science Foundation (Grant GEO0909515), and the United States Department of Agriculture/Agricultural Research Service (Ogallala Aquifer Initiative).

References

[1] Abramowitz M, Stegun IA. Handbook of mathematical functions. New York: Dover Publications; 1972.
[2] Ahring TS, Steward DR. Groundwater surface water interactions and the role of phreatophytes in identifying recharge zones. Hydrol Earth Syst Sci 2012;16:4133–42.
[3] Aistrup JA, Kulcsar L, Beach S, Mauslein J, Steward DR. Hyper-extractive economies in the U.S.: a coupled-systems approach. Appl Geogr 2013;37:88–100.
[4] Allen, AJ. Analytic element modeling of the high plains aquifer: non-linear model optimization using Levenberg–Marquardt and particle swarm algorithms, M.S. Civil Engineering, Kansas State University, Manhattan, Kansas, 2012.
[5] Bakker M. Hydraulic modeling of riverbank filtration systems with curved boundaries using analytic elements and series solutions. Adv Water Resour 2010;23:813–9.
[6] Bandilla KW, Janković I, Rabideau AJ. A new algorithm for analytic element modeling of large-scale groundwater flow. Adv Water Resour 2007;30:446–54.
[7] Barnes R, Janković I. Two-dimensional flow through large number of circular inhomogeneities. J Hydrol 1999;226:204–10.
[8] Carslaw HS, Jaeger JC. Conduction of heat in solids. second edition. Oxford: Oxford University Press; 1959.
[9] Cederstrand, JR, Becker, MF. Digital map of base of aquifer for the high plains aquifer in parts of Colorado, Kansas, Nebraska, New Mexico, Oklahoma, South Dakota, Texas and Wyoming, Open File Report 98–393, U.S. Geological Survey, 1998a (available online at pubs.usgs.gov/of/1998/of98-393).
[10] Cederstrand, JR, Becker, MF. Digital map of hydraulic conductivity for the high plains aquifer in parts of Colorado, Kansas, Nebraska, New Mexico, Oklahoma, South Dakota, Texas and Wyoming, Open File Report 98–548, U.S. Geological Survey, 1998b (available online at pubs.usgs.gov/of/1998/of98-548).
[11] Cederstrand, JR, Becker, MF. Digital map of predevelopment water levels for the high plains aquifer in parts of Colorado, Kansas, Nebraska, New Mexico, Oklahoma, South Dakota, Texas and Wyoming, Open File Report 99–264, U.S. Geological Survey, 1999 (available online at pubs.usgs.gov/of/1999/ofr99-264).
[12] Craig JR. Analytical solutions for 2D topography-driven flow in stratified and syncline aquifers. Adv Water Resour 2008;31:1066–73.
[13] Craig JR, Janković I, Barnes R. The nested superblock approach for regional-scale analytic element models. Groundwater 2006;44:76–80.
[14] Dagan G. Models of groundwater flow in statistically homogeneous porous formations. Water Resour Res 1979;15:47–63.
[15] Dagan G. Analysis of flow through heterogenous random aquifers by the methods of embedding matrix 1. Steady flow. Water Resour Res 1981;17:107–21.
[16] Fitts CR. Modeling aquifer systems with analytic elements and subdomains. Water Resour Res 2010;46:W07521.
[17] Fourier, JBJ. Mémoire sur la propagation de la chaleur dans les corps solides, Nouveau Bulletin des Sciences par la Société Philomathique de Paris, 1808, pp.112–116 (reprinted in Oeuvres complètes, tome 2. pp. 215–221).
[18] Gutentag, ED, Heimes, FJ, Krothe, NC, Luckey, RR, Weeks, JB. Geohydrology of the high plains aquifer in parts of Colorado, Kansas, Nebraska, New Mexico, Oklahoma, South Dakota, Texas and Wyoming, Professional Paper 1400-B, U.S Geological Survey, 1984.
[19] Haitjema HM. Analytic element modeling of groundwater flow. San Diego: Academic Press; 1995.
[20] Hansen, CV. Estimates of freshwater storage and potential natural recharge for principal aquifers in Kansas, Water resources investigations 87–4230, U.S Geological Survey, 1987.
[21] Janković I, Barnes RJ. High-order line elements in modeling two-dimensional groundwater flow. J Hydrol 1999;226:211–23.
[22] Janković I, Barnes RJ. Three-dimensional flow through large numbers of spheroidal inhomogeneities. J Hydrol 1999;226:224–33.
[23] Janković I, Fiori A, Dagan G. Flow and transport in highly heterogeneous formations: 3. Numerical simulations and comparison with theoretical results. Water Resour Res 2003;39:SBH16:1–13.
[24] Janković I, Steward DR, Barnes RJ, Dagan G. Is transverse macrodispersivity in three-dimensional transport through isotropic heterogeneous formation equal to zero? A counterexample. Water Resour Res 2009;45:W08415:1–10.
[25] Kacimov AR, Obnosov YV, Yakimov ND. Groundwater flow in a medium with parquet-type conductivity distribution. J Hydrol 1999;226:242–9.
[26] Knight JH, Philip JR. Exact solutions in nonlinear diffusion. J Eng Math 1974;8:219–27.
[27] Liu, G, Wilson, B, Whittemore, D, Jin, W, Butler, J, Jr. Ground-water model for Southwest groundwater management district no. 3, Open File Report 2010–18, Kansas Geological Survey, University of Kansas, Lawrence, KS, 2010.
[28] McDonald, MG, Harbaugh, AW. A modular three-dimensional ground-water flow model, Techniques of water-resource investigation 06–A1, USGS, U.S. Government Printing Office, Washington, 1988.
[29] Moon P, Spencer DE. Field theory for engineers. Princeton, New Jersey: D. Van Nostrand Company, Inc.; 1961.
[30] Moon P, Spencer DE. Field theory handbook including coordinate systems differential equations and their solutions. Berlin: Springer-Verlag; 1961.
[31] Obnosov YV. Exact solution of a boundary-value problem for a rectangular checkerboard field. Proc R Soc Lond Ser A Math Phys Eng Sci 1996;452:2423–42.
[32] Peterson TE. Eliminating Gibb's effect from separation of variables solutions. SIAM Rev 1998;40:324–6.
[33] Steward DR. Groundwater response to changing water-use practices in sloping aquifers. Water Resour Res 2007;43:W05408:1–12.
[34] Steward DR, Ahring T. An analytic solution for groundwater uptake by phreatophytes spanning spatial scales from plant to field to regional. J Eng Math 2009;64:85–103.
[35] Steward DR, Bernard EA. The synergistic powers of AEM and GIS geodatabase models in water resources studies. Ground Water 2006;44:56–61.
[36] Steward, DR, Bruss, PJ, Yang, X, Staggenborg, SA, Welch, SM, Apley, MD. Tapping unsustainable groundwater stores for agricultural production in the high plains aquifer of Kansas from the predevelopment era to 2110. In: Proceedings of the national academy of sciences of the United States of America in review, 2013.
[37] Steward DR, Le Grand P, Janković I, Strack ODL. Analytic formulation of Cauchy integrals for boundaries with curvilinear geometry. Proc R Soc Lond Ser A Math Phys Eng Sci 2008;464:223–48.
[38] Steward DR, Peterson JM, Yang X, Bulatewicz T, Herrera-Rodriguez M, Mao D, Hendricks N. Groundwater economics: an object oriented foundation for integrated studies of irrigated agricultural systems. Water Resour Res 2009;45:W05430:1–15.
[39] Steward DR, Yang X, Chacon S. Groundwater response to changing water-use practices in sloping aquifers using convolution of transient response functions. Water Resour Res 2009;45:W02412:1–13.
[40] Stokes GG. Mathematical and physical papers, vol. 1. London: Cambridge University Press; 1880.
[41] Strack ODL. Groundwater mechanics. Englewood Cliffs, NJ: Prentice Hall; 1989.
[42] Strack ODL. Theory and applications of the analytic element method. Rev Geophys 2003;41(1):1–19.
[43] Strack ODL, Janković I, Barnes RJ. The superblock approach for the analytic element method. J Hydrol 1999;226:179–87.
[44] Suribhatla R, Bakker M, Bandilla K, Janković I. Steady two-dimensional groundwater flow through many elliptical inhomogeneities. Water Resour Res 2004;40:W042002:1–10.
[45] Thiem G. Hydrologische methoden. Leipzig: J.M. Gebhardt; 1906.
[46] USDA, National agricultural statistics service, Kansas state and county data. In: Census of agriculture, AC-07-A-16, United States Department of Agriculture, Washington, DC, vol. 1; 2007.